Xyloglucan-cellulose nanocrystal-chitosan double network hydrogels for soft actuators

Nadège Leray, Malika Talantikite, Ana Villares, Bernard Cathala

Xyloglucan-cellulose nanocrystal-chitosan double network hydrogels for soft actuators

Nadège Leray, Malika Talantikite, Ana Villares, Bernard Cathala*

UR1268 BIA, INRAE, 44300, Nantes, France

* : corresponding author

email : Bernard.cathala@inrae.fr

ABSTRACT

Hydrogels are materials consisting in a three-dimensional hydrophilic polymer network swollen by a large amount of water. An efficient strategy to elaborate hydrogels consists in establishing double polymer networks in order to achieve high strengthening effect associated with other properties such as transparency or tailored swelling capacities. In this work, we prepared cellulose nanocrystals (CNC)-based hydrogels with double network architecture. The first network, formed by CNC and xyloglucan (XG), takes advantage of entropic adsorption of XG on the CNC surface while the second network relies on electrostatic interactions between cationic Chitosan (Chi) and anionic CNC. Hydrogels with different compositions were successfully prepared. Their rheological properties, stability and swelling capacities in acidic and alkaline solutions were evaluated. Internal organizations of hydrogels were investigated by fluorescence microscopy after polymer labelling and polarized optical microscopy (POM). Finally, hydrogels demonstrated excellent mechanical properties and tuneable swelling capacities that can be leveraged for the implementation of bilayer actuators. Therefore, we further prepared films composed of two hydrogels layers, each one containing a different XG/CNC ratio. Bilayered

films bended in water due to the asymmetric swelling of layers and the extent of bending can be modulated by the XG/CNC ratio.

Keywords: xyloglucan, cellulose nanocrystals, chitosan, hydrogel, swelling, actuator.

1. Introduction

Hydrogels have attracted much attention due to their ability to hold large amounts of water. They have been studied for decades as they found applications in various fields including medicine, pharmaceutics, cosmetics, domestic uses and personal care (Patel & Thareja, 2022; T. Zhu et al., 2019). Hydrogels are composed of three-dimensional polymer networks that exhibit outstanding features such as high water absorption, transparency and good mechanical properties among many others. During last two decades, research has focused on natural hydrogels to gradually replace synthetic hydrogels. Biopolymers have demonstrated a great potential, particularly, polysaccharides are excellent candidates thanks to the presence of a high number of hydrophilic groups (hydroxyl groups and others). Different polysaccharides have demonstrated gel-like behavior, such as alginate, carrageenan, chitosan, cellulose or starch (Chang & Zhang, 2011; Coviello, Matricardi, Marianecci, & Alhaique, 2007; Patel & Thareja, 2022; T. Zhu et al., 2019). Nanocelluloses have also arisen as outstanding components of hydrogels (Du et al., 2019). Indeed, cellulose nanocrystals (CNC), which are obtained by acid hydrolysis of the cellulose fiber, provide excellent mechanical properties thanks to their rigid nature and rod-like shape (Eichhorn, 2011; Moreau, Villares, Capron, & Cathala, 2016). The specific association of cellulose with certain hemicelluloses, such as xyloglucan (XG), allows controlling the swelling behavior (Villares, Bizot, Moreau, Rolland-Sabate, & Cathala, 2017), and results in gel-like dispersions (Talantikite, Beury, Moreau, & Cathala, 2019; Talantikite, Gourlay, Le Gall, & Cathala, 2019; Talantikite et al., 2021). The XG/CNC hydrogels are stabilized by hydrogen bonds and dispersive forces, which allows the breakdown and re-formation of the gel under shearing. However, hydrogen bonds do not confer enough stability to the network and the XG/CNC hydrogels are mechanically weak and loose its shape under shear forces (Talantikite,

Gourlay, et al., 2019). One strategy to obtain more mechanically efficient networks is the formation of semipermanent junction points by interanchored long chains. In this field, the formation of interpenetrating networks significantly improves the mechanical properties, and the hydrogel stability (K. J. De France, Cranston, & Hoare, 2020; Kevin J. De France, Hoare, & Cranston, 2017). The physical interlocking of two networks, known as the double or interpenetrating network, creates junction points that stabilize the hydrogel and favor water uptake.

In this work, we took advantage of the specific interactions between polysaccharides and nanocellulose to prepare all biobased hydrogels. Hydrogels were produced by a sequential two-step process, firstly creating the XG/CNC network, and then cross-linking a second network of chitosan (Chi) within the first. The specific interaction between XG and CNC provides the physical properties such as water uptake and mechanical resistance, and the electrostatic interaction between the positive charge of Chi and anionic CNC facilitated the interaction between the two networks. We obtained highly swollen and transparent hydrogels, showing good mechanical resistance. By changing the XG/CNC ratio, we succeeded in tuning the hydrogel properties in terms of water uptake and mechanical properties with a simple, efficient and green process. The formation of anisotropic structures, such as successive layers showing different swelling behavior and/or mechanical properties may trigger shape changes and motion, which is the mechanism of actuation (McCracken, Donovan, & White, 2020; Shang, Le, Zhang, Chen, & Theato, 2019). Soft actuators from biopolymers have attracted much attention thanks to their environmentally friendly properties and the possibility to tune their response by non-covalent interactions (Wu et al., 2013; Zhao et al., 2021; Q. Zhu et al., 2020). In this field, polysaccharides have demonstrated to be excellent candidates because of their tunable water

swelling arising from their structural and chemical versatility (Chemin, Beaumal, Cathala, & Villares, 2020; W. Chen, Sun, Biehl, & Zhang, 2022). Therefore, in this study we focused on the impact of hydrogel composition (i.e. XG/CNC ratio) on their mechanical properties and water uptake. The different behavior of the XG/CNC assemblies permitted to fabricate bilayer actuators driven by the asymmetric swelling of layers when the films are immersed in water.

2. Materials and methods

2.1. Materials

Cellulose nanocrystals (CNC) were purchased from CelluForce (Canada). CNC were obtained by acid hydrolysis of wood pulp and according to product specification, purity = 100% surface charge density = 0.023 mmol g^{-1} (by conductivity), crystalline fraction = 0.88 (by XRD), crystallite diameter = 2.3–4.5 nm (by AFM), crystallite length = 44–108 nm (by AFM), pH (dispersion in water) = 6–7. Xyloglucan (XG), M_w = 800 kDa, from tamarin seed gum, was purchased from DSP Gokyo Food and Chemical (Japan). Chitosan (Chi) medium molecular weight, Brookfield viscosity 200-800 cP, was purchased from Sigma Aldrich. Rhodamine B isothiocyanate (RBITC) was purchased from Sigma Aldrich. Acetic acid and dimethylsulfoxyde (DMSO) were purchased from Merck.

2.2 CNC, XG and Chitosan solutions/dispersions preparation

CNC dispersion was prepared in Milli-Q water at a final concentration of 2 % *w/w*. Dispersion was vigorously stirred during 24 h and finally sonicated. XG solution was prepared in Milli-Q water at final concentration of 2 % *w/w*, and vigorously stirred during 24 h. Chitosan solution at 0.1 % *w/w* was prepared in acetic acid 1%, at room temperature and vigorously stirred for 24 h.

2.3. Fluorescence labelling of chitosan

RBITC-labelled chitosan was synthesized by the reaction between isothiocyanate group of RBITC and amino group of chitosan. Chitosan (1 g) was dissolved at 1% in 0.1 M acetic acid. RBITC (7.5 mg) dissolved in 20 mL DMSO was add to chitosan solution. The mixture was stirred for 3 h, in dark, at room temperature. Labelled-chitosan was precipitated by addition of NaOH. Labelled-chitosan was centrifuged and washed with ultra-pure water until no free RBITC was detected in supernatant. Chitosan-RBITC was solubilized in acetic acid 1% and dialyzed against ultra-pure water during 3 days in dark.

2.3. Films and hydrogel bilayers fabrication

5 mL of CNC and XG were mixed at different XG/CNC ratios (R1, R0.5 and R0.2) with same final polysaccharide concentration (1.2 % *w/w*) and vortexed to obtain a homogeneous gel solution. CNC and XG solution concentrations for the different ratio were : R=0.2 [CNC] = 1 % *w/w*; [XG] = 0.2 % *w/w*; R=0.5 [CNC] = 0.8 % *w/w*; [XG] = 0.4 % *w/w*; R=1 [CNC]= 0.6 % *w/w*; [XG] = 0.6 % *w/w*. Gels were casted into Petri dishes (diameter 3 cm), and 2.5 mL chitosan at 0.1 % *w/w* was added above the gel. After floated gel in chitosan during one night, chitosan supernatant was removed, and the gel was dried at room temperature for 24 h. Film thickness was measured by a micrometer. The three different bilayer films by the successive deposition of XG/CNC/Chi hydrogels at the selected XG/CNC ratios: R0.5/R0.2, R1/R0.2 and R1/R0.5. The first hydrogel layer was casted into a Petri dish and the second one was immediately and carefully put on the top of the first one. Then chitosan was added to cross-link the bilayered films.

2.4. Transmittance

UV-visible spectra were obtained from films placed directly in a SPECORD S 600 spectrometer (Analytik Jena GmbH). All spectra were recorded using WinASPECT software set to absorbance mode after 10 accumulations and scanning from 182 to 1019 nm.

2.5. Rheology

Rheological measurements were performed using a stress-controlled rheometer AR-2000 (TA Instruments) equipped with a plane geometry (20 mm diameter). The storage (*G'*) and loss (*G''*) moduli were measured at different frequencies range (100 to 0.01 Hz). The imposed stress was chosen within the linear response regime. Temperature was controlled using the Peltier and set at 20 °C for all measurements. Samples were covered with paraffin oil to prevent sample evaporation. Samples were shaped to fit the geometry. Three samples were used for each measurement; they displayed reproducible behaviour and values.

2.6. Water uptake of films

The obtained hydrogels were placed in water, or in acid or alkaline pH solutions, to swell until equilibrium at room temperature. The swelling degree was calculated by weighing the samples before and after immersing in acetate (50 mM, pH 3.5) and carbonate buffer (50 mM, pH 10.5). The mass swelling percentage was calculated using the following expression:

$$S\ (\%) = \frac{m_t - m_0}{m_0}\ 100 \qquad (1)$$

Where m_0 and m_t are the weights of the dry gel at time 0 and the swollen gel at time *t*, respectively.

For the actuation tests, films were immersed in water, and the bending curvature was determined by recording movies during the water uptake, and periodically extracting pictures. Films were fixed with a binder clip leaving a free length of approximately 30 mm.

2.7. Polarized optical microscopy (POM)

Polarized optical microscopy (POM) was performed using an upright Olympus System Microscope Model BX51, with crossed polarizers and a 530 nm retardation plate (U-TP530). Digital images were taken of samples between the microscopy slide and the cover glass using a Sony XCD-SX90CR charge-coupled device camera.

2.8. Confocal microscopy

Films containing rhodamine-labelled Chitosan were imaged by confocal microscopy (Leica TCS-SP2). Confocal images of the microcapsules were acquired with LSM-510 UV−Vis equipped with 63 × 1.2 water immersion objectives (Zeiss, Germany). Excitation/emission wavelengths were 530/566 nm.

3. Results and Discussion

3.1. Preparation of XG/CNC/Chi hydrogels and evaluation of their optical properties.

XG adsorption on cellulose surface has been reported for decades and has been more recently identified as an entropy driven process (Tobias Benselfelt et al., 2016; Kishani, Benselfelt, Wagberg, & Wohlert, 2021). According to the XG/CNC ratio, the surface crowding can be tailored to form a variable proportion of loops and tails as demonstrated by enzymatic hydrolysis of XG/CNC complexes displaying various mass ratios (Dammak et al., 2015). Indeed, the trains are defined as the part of the polymer that are adsorbed in contact with surface, while the loops and the tails correspond to the parts of the polymers that are not directly attached to the surface (Tobias Benselfelt et al., 2016), being the tails the end parts of the polymer chains. Thus the loops and tails are accessible to enzymes while the trains are not. At low XG/CNC ratio, the surface availability is high and leads to XG adsorption in an extended conformation while at higher XG/CNC ratio, loops and tails are more frequent due to the surface crowding. These results can be explained by the fast adsorption kinetics of XG on the cellulose surface and the

slow rate of the desorption that leads to almost irreversible adsorption (Park & Cosgrove, 2015; Villares, Moreau, Dammak, Capron, & Cathala, 2015). In this work, the rationale was the base of the choice of the XG/CNC ratio used. Indeed, the limit of the CNC surface saturation by XG was found to be in the range of 250 µg of XG per mg of CNC, i.e. 0.25 *w/w* ratio (Dammak et al., 2015). We therefore studied three different XG/CNC ratios for the hydrogel fabrication. The lowest one (XG/CNC 0.2 *w/w*; R0.2) corresponded to a XG concentration slightly lower than the saturation limit so that CNC surface will be not fully crowded and XG may adopt an extended conformation. Moreover, since the amount of CNC surface is lower than XG available, XG chains can interact more easily with two CNC leading to the cross-link of the nanorods. The two other XG/CNC ratios, 0.5 *w/w* (R0.5) and 1.0 *w/w* (R1), were clearly higher than the saturation limit and corresponded to the formation of loops and tails due to surface crowding. In this case, XG chains are more accessible as demonstrated by the enzymatic degradation (Dammak et al., 2015).

For all the studied ratios, when the total biopolymer concentration (XG + CNC) is high enough (> 1% *w/w*), gel formation occurs (Talantikite, Gourlay, et al., 2019; Talantikite et al., 2021). Indeed, in solution, the adsorption of XG on stiff CNC increases the effective hydrodynamic volume of XG/CNC complexes, compared to CNC alone, leading to gel formation through steric repulsion and transient network formation between XG chains (de Freitas et al., 2015; Talantikite, Gourlay, et al., 2019). Similar gelation process was observed for other CNC adsorbing polymers (Hu, Cranston, Ng, & Pelton, 2014).Variation of XG/CNC ratio influenced the gel strength due to the modification of CNC cross-linking and XG/XG chains interaction extent (Talantikite, Gourlay, et al., 2019; Talantikite et al., 2021). Nevertheless, the interaction strength between XG chains is weak leading to hydrogels with poor mechanical properties

185 (Talantikite, Gourlay, et al., 2019). A general strategy to achieve hydrogel strengthening consists
186 in the elaboration of double network architectures (Q. Chen, Chen, Zhu, & Zheng, 2015). This
187 approach has been successfully implemented for nanocellulose-based materials either by using
188 ionic or covalent cross-linking (T. Benselfelt, Engstrom, & Wagberg, 2018; K. J. De France et
189 al., 2020). Similarly, our strategy relies on electrostatic interactions and takes advantage of
190 interplay capacities of negative sulfate groups present on CNC with polycations. Among bio-
191 based polycations, chitosan has been widely used for different materials preparation including
192 hydrogels and was also found to be able to cross-link cellulosic substrates such as paper or
193 nanocellulose (Lindstrom, Wagberg, & Larsson, 2005; Toivonen et al., 2015).
194 Fig. 1a shows the scheme of the XG/CNC/Chi hydrogels fabrication. Hydrogels were prepared
195 by first mixing XG and CNC at the appropriate ratio (R0.2, R0.5 and R1) at a constant total dry
196 weight (XG + CNC) of 1.2 % *w/w*. The mixture was thoroughly stirred to achieve homogeneity.
197 Indeed, Talantikite et al. (Talantikite, Gourlay, et al., 2019) demonstrated that XG/CNC gels can
198 be easily broken by shearing and then reformed instantaneously. These self-healing properties
199 rely on transient no-covalent interactions between XG chains (de Freitas et al., 2015). The gels
200 were thereafter molded in a Petri dish to achieve cross-linking. Chi solution (0.1 % *w/w*) was
201 added on the XG/CNC dispersion. Several chitosan concentrations were tested (data not shown)
202 and since concentration have been found to have no effect on swelling and mechanical properties
203 (data not shown), 0.1 %*w/w* concentration was chosen. After Chi addition, for all the XG/CNC
204 ratios, hydrogel shrinkage was visually observed, suggesting that water was removed. This
205 behavior has been previously observed in the fabrication of CNC/Chi multilayers monitored by
206 quartz crystal microbalance with dissipation (QCM-D) (Lombardo, Cathala, & Villares, 2021).
207 These studies revealed that the adsorption of Chi onto CNC yielded lower adsorbed hydrated

mass than in the case of XG, which pointed at a shrinking effect of Chi mediated by the electrostatic interaction between CNC and Chi. The strong interaction could therefore expel water molecules and counter-ions from the CNC surface by an entropy-driven process (Lombardo & Thielemans, 2019), which stabilized the hydrogel and provided the self-supporting properties.

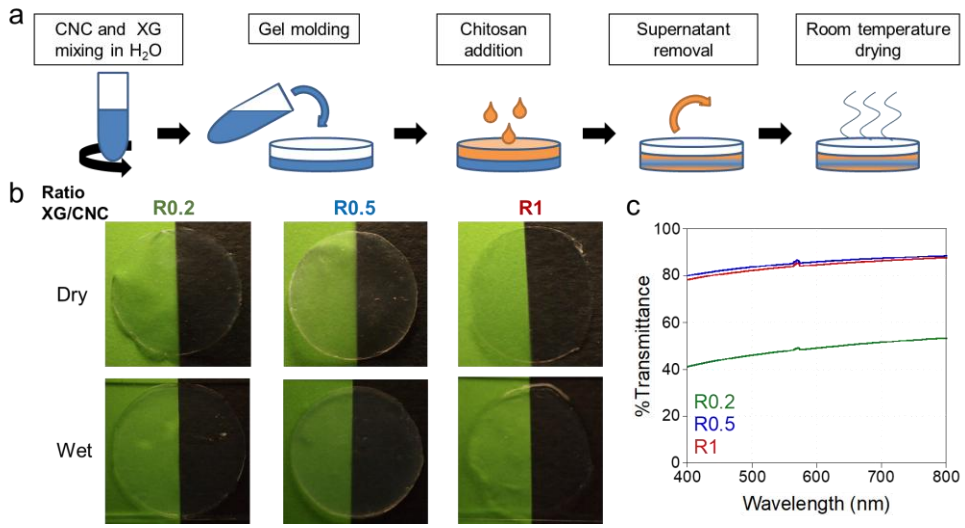

Fig. 1. (a) Schematic illustration of the preparation of XG/CNC/Chi hydrogels; (b) photography showing the transparency of the hydrogels; and (c) transmittance values of hydrated hydrogels in the range of 400-800 nm for the three XG/CNC/Chi hydrogels studied, R0.2, R0.5 and R1.

The optical properties were examined by transmittance measurements of dry and hydrated films. As-prepared films were highly transparent, smooth and flexible (**Fig. *1***b). When hydrogels were rehydrated, transmittance increased in all cases, being more noticeable in the case of R0.2 XG/CNC/Chi hydrogels (Table 1). For the higher XG/CNC ratios (R0.5 and R1) the transmittance was 80% whereas for the lower XG/CNC ratio, the transmittance was around 40% (**Fig. *1***c and Table *1*). This lower transmittance suggested the presence of light-scattering aggregates. This difference between R0.2 and the two other systems could be ascribed to the

association between CNC mediated by XG chains when available CNC surfaces are larger than the amount of XG available to cover all CNC surfaces. This might result in tight contact between CNC forming large particles and therefore less transparency.

Table 1 : Characteristics of XG/CNC/Chi hydrogels in terms of water uptake ratio, transmittance, mechanical properties and thickness

Composition	Water uptake ratio (g/g)		Transmittance (% at λ= 550 nm)		Mechanical properties		Thickness	
XG/CNC ratio	pH 3	pH 10	Dry	Wet	G' (kPa)	G'' (kPa)	Dry (μm)	Wet (μm)
R0.2	4.9	3.5	31	41	68.4	5.1	91± 18	812 ± 93
R0.5	10.4	6.1	80	87	5.1	0.3	64 ± 7	653 ± 78
R1	19.7	14.7	80	84	1.8	0.1	31 ± 5	700 ± 140

3.2. Mechanical properties

The dynamic mechanical properties of XG/CNC/Chi hydrogels were investigated by measuring the frequency dependence of the storage (*G'*) and loss (*G''*) moduli (**Fig.*2***, Table *1*). For the three studied XG/CNC ratios, R0.2, R0.5 and R1, the storage modulus was always higher than the loss modulus (*G'>G''*), which indicated a gel and elastic-like behavior (Pääkkö et al., 2007). The values of both storage and loss moduli were particularly high in comparison with CNC/polymer hydrogels (Hynninen et al., 2018; Talantikite, Gourlay, et al., 2019).

Results showed clear differences on the rheological behavior depending on the XG/CNC ratio. Thus, the values of both *G'* and *G''* decreased when the XG/CNC ratio increased, reflecting a significant increase of rigidity when the amount of CNC increased. Nevertheless, the decrease in *G'* and *G''* was not correlated to the CNC concentration, which revealed the role of the XG conformation on the mechanical properties. These results clearly showed the transition to a different regime above 0.25 *w/w* (Dammak et al., 2015). Thus, the low XG concentration (R0.2), which adsorbs in an extended conformation on the CNC surface, provided rigidity and cross-linking between CNC to the XG/CNC/Chi hydrogels whereas the XG conformation as loops and tails prevailing for the higher XG concentrations (R0.5 and R1) provided more flexibility. Moreover, the low coverage of surface by XG might also favor interactions between CNC sulfate charges and Chi charges leading to a reinforcing effect.

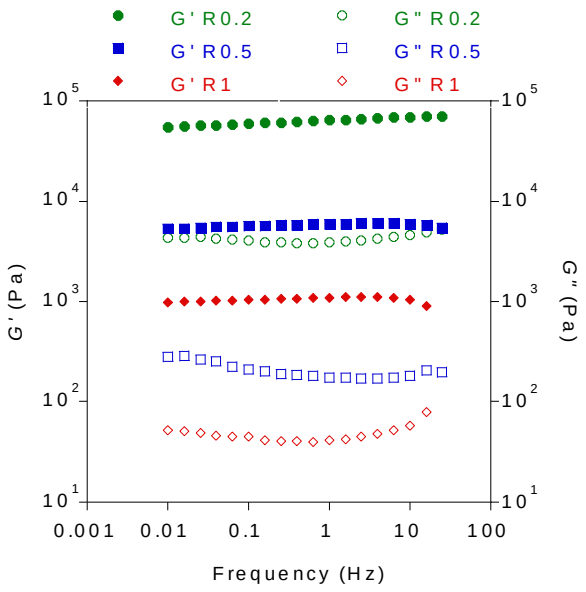

Fig.2. The storage modulus (*G'*) and the loss modulus (*G''*) as a function of the frequency for the three XG/CNC/Chi hydrogels studied, R0.2, R0.5 and R1, at 20 °C.

3.3. Swelling properties of hydrogels

The swelling properties of the XG/CNC/Chi hydrogels were determined by the water uptake in two different buffers, i.e. acetate (pH 3.5) and carbonate (pH 10.5) (**Fig. 3**). Similarly to mechanical properties, the swelling behavior was significantly influenced by the XG/CNC ratio. Thus, as the XG/CNC ratio increased, the hydrogels adsorbed more water. In all cases, absorption is extremely fast and equilibrium was reached after few hours of immersions. All hydrogels displayed high stability in the two pH conditions since the gels retained their full integrity for weeks (**Fig. 3**).

Swelling involves the diffusion of water molecules into the gel matrix and the subsequent polymer chain relaxation within the hydrogel. The capacity of the hydrogel for water adsorption depends on the interactions between the biopolymers. Swelling can be explained in terms of equilibrium swelling pressure that is constituted of the contribution from interaction of water with the polymers forming the gels, the osmotic pressure due to charged groups of polymer constituents and the pressure due to the resistance of the gel network (T. Benselfelt et al., 2018; Flory, 1953). If the first two pressures are higher than the later, the gel will be dissolved whereas if the pressure generated by the network resistance dominates, the swelling will be limited. Therefore, the formation of tight entanglements results in low swelling whereas loose and flexible networks show high water uptake. In the case of low XG/CNC ratio (R0.2), the formation of tight contacts between cellulose and xyloglucan in association with potentially more efficient interaction between Chi and CNC charges resulted in less swollen networks. As the XG/CNC ratio increases (R0.5 and R1), the formation of XG loops and tails on the CNC surface, as well as the present of some unbound XG chains for the highest ratio, facilitated water adsorption. These results are in agreement with previous studies showing that the XG adsorption onto CNC forming loops and tails resulted in higher water uptake, and the hydration of XG

chains increased significantly their accessibility and the thickness of CNC/XG/CNC multilayer films (Villares et al., 2017). The thicknesses of hydrogels were measured before and after drying (Table 1). For the three hydrogels studied, the thickness increased between 800-2000%, which demonstrated the hydrogel character of the XG/CNC/Chi systems.

Finally, it is necessary to underline the difference of swelling observed in the acetate buffer and the carbonate buffer. The swelling was more important at acidic pH due to the protonation of the amine groups of the chitosan which reinforced the electrostatic repulsion between the chitosan chains and increased the hydrophilicity of the hydrogels.

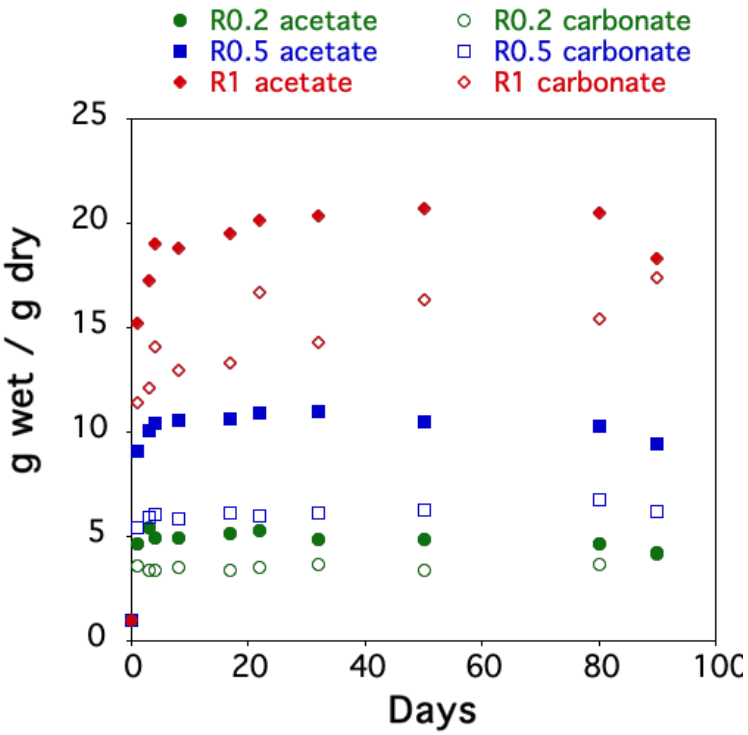

Fig. 3. Variation of water uptake with time in acetate (pH 3.5) and carbonate buffers (pH 10.5) for the three XG/CNC/Chi hydrogels studied, R0.2, R0.5 and R1.

3.4. Internal architecture of hydrogels

CNC are known to self-assemble into chiral nematic liquid crystal phases with twisted helicoidal organization. This self-assembled organization is characterized by a specific fingerprint pattern. This pattern is present when the band spacing is large enough to be resolved in the optical microscope (Revol, Bradford, Giasson, Marchessault, & Gray, 1992). CNC/XG/Chi hydrogels have been observed under cross-polarized light and birefringence has been observed, but finger print pattern cannot be identified (**Fig. 4**). Hydrogel microstructures displayed anisotropic zones as demonstrated by the birefringence indicating certain level of CNC organization but not as highly organized as in chiral nematic phases. It is likely that the anisotropic zones visualized by POM are constituted of XG and CNC and not only by highly organized and phase separated CNC. Hydrogels microstructures were also revealed by fluorescence microscopy (**Fig. *4***). For this purpose, Chi was labelled with rhodamine B. XG/CNC hydrogels were then cross-linked with rhodamine-labelled Chi and were then further imaged to reveal the domains accessible to Chi.

Both POM and fluorescence images reported in **Fig. *4*** indicate that the microstructures of hydrogels were strongly influenced by the XG/CNC ratio. For the lowest ratio (R 0.2), both microscopy modalities clearly indicated the formation of small size domains. The POM images showed different colored domains suggesting varying preferential orientations and/or changes in material density from one domain to another. Also, different fluorescence intensities were clearly detected, indicating that some areas appeared richer in labeled Chi than others that seemed less accessible. This result was consistent with the formation of CNC-rich domains that appeared aggregated (and thus less accessible) due to the lack of XG that defaults to the amount of CNC surface area available. When the XG/CNC ratio increased, the microstructure of the hydrogel became more homogeneous. In the case of R0.5 ratio, regions with different birefringence were

clearly visible while in the case of R1 ratio, large areas displayed the same birefringence pattern. Similarly, for R1 ratio, fluorescent labelling became completely homogeneous. These results suggested that CNC, XG and Chi were uniformly distributed at the highest XG/CNC ratio and no phase separation occurred at least at the microscale.

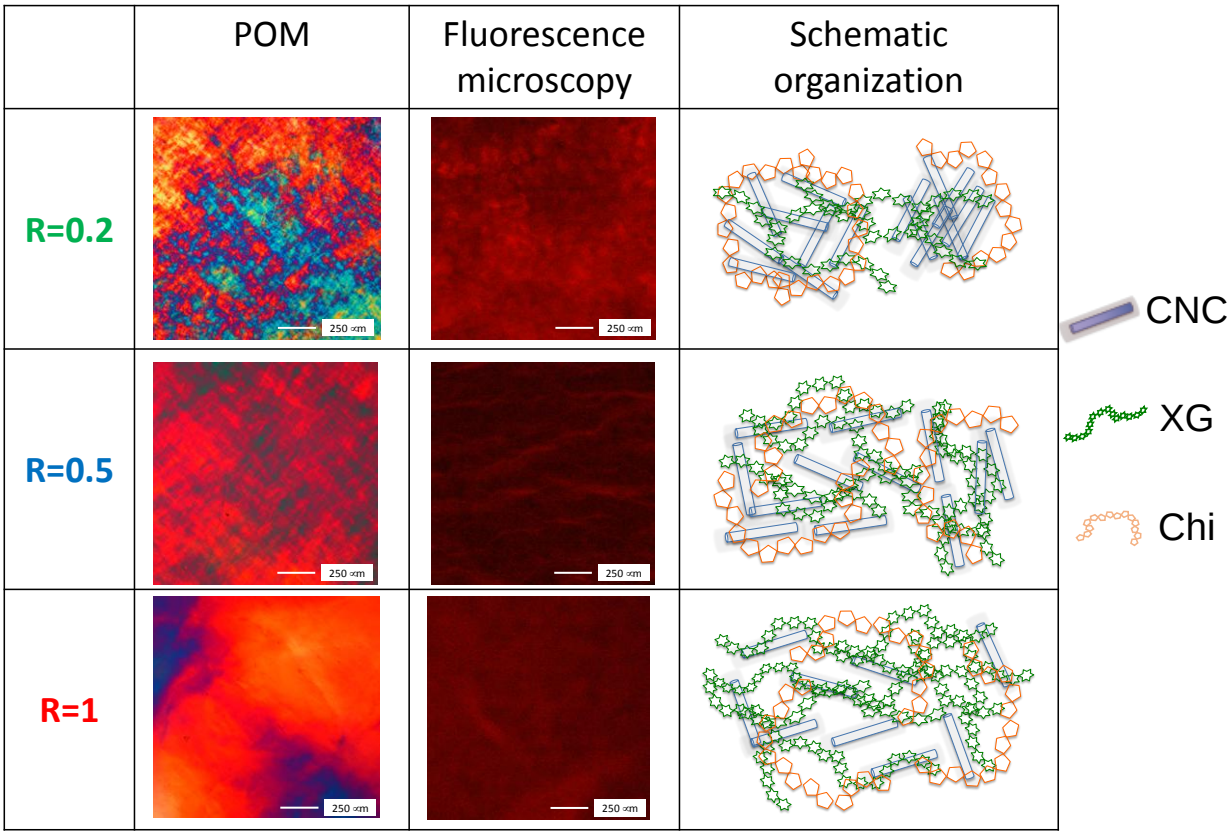

Fig. 4. Polarized optical microscopy images (crossed polarizers, 530 nm red wave plate); confocal microscopy images of hydrogels fabricated with rhodamine-labelled Chi; and schematic representation of the arrangement of biopolymers in the hydrogels for the three XG/CNC/Chi systems studied, R0.2, R0.5 and R1. XG and Chis are represented by a green and yellow strands respectively, CNC are represented by purple rods surrounded by pink light rods representing the electrostatic double layer.

Fig. *4* depicts an illustration of the biopolymer arrangement within the hydrogel. When XG concentration was low (R0.2), XG adsorbed in an extended conformation on the CNC surface, that favored the close interaction between CNC, and therefore, the formation of compacted networks/aggregates consistent with le lowest transparency observed (**Fig. *1*)**. Chi stabilized the system, forming more rigid hydrogels yielding higher mechanical properties. The tight contact between biopolymers made therefore difficult to accommodate many water molecules, and the water uptake of XG/CNC/Chi R0.2 hydrogels was low compared to the other XG concentrations. When the XG concentration increased (R0.5), there was a transition to a regime XG forming loops and tails on the CNC surface, resulting in a more swollen and flexible network, where Chi interpenetrated and formed junctions that reinforced and stabilized the hydrogel. Accordingly, transparency increased since the CNC are better dispersed, and swelling increased also due to the lowest resistance of the network (less XG cross linking) and simultaneously the mechanical properties decreased. The higher XG concentration (R1) resulted in a highly swollen hydrogel where the lower CNC concentration prevented the formation large CNC rich domains. XG showed a uniform distribution within the hydrogel and increase the water affinity and swelling capability while lowering the mechanical properties.

3.5. Towards the implementation of soft actuators

We took advantage of the different rheological and swelling properties to fabricate water swelling-driven actuators. We prepared three different bilayer films by the successive deposition of XG/CNC/Chi hydrogels at the selected XG/CNC ratios: R0.5/R0.2, R1/R0.2 and R1/R0.5. Water uptake resulted in a volume increase; therefore, the combination of two layers differing in their swelling behavior resulted in an asymmetric expansion of the film. Depending on the

geometry of the film, different responses can be obtained, such as bending, twisting, or self-rolling. Square-shaped films (10×10 cm) were cut into rectangles of 5×35 mm. The film thickness was significantly influenced by the film composition, varying from 95 µm for the R1/R0.5 film, to122 µm for the R1/R0.2 film, and to 155 µm for the R0.5/R0.2. When the films were immersed in water, they changed their shape from straight (time 0) to bended, reaching a maximum curvature over 30 min. **Fig. 5** shows the photographs of the films when they were immersed in water at time 0 and after 30 min.

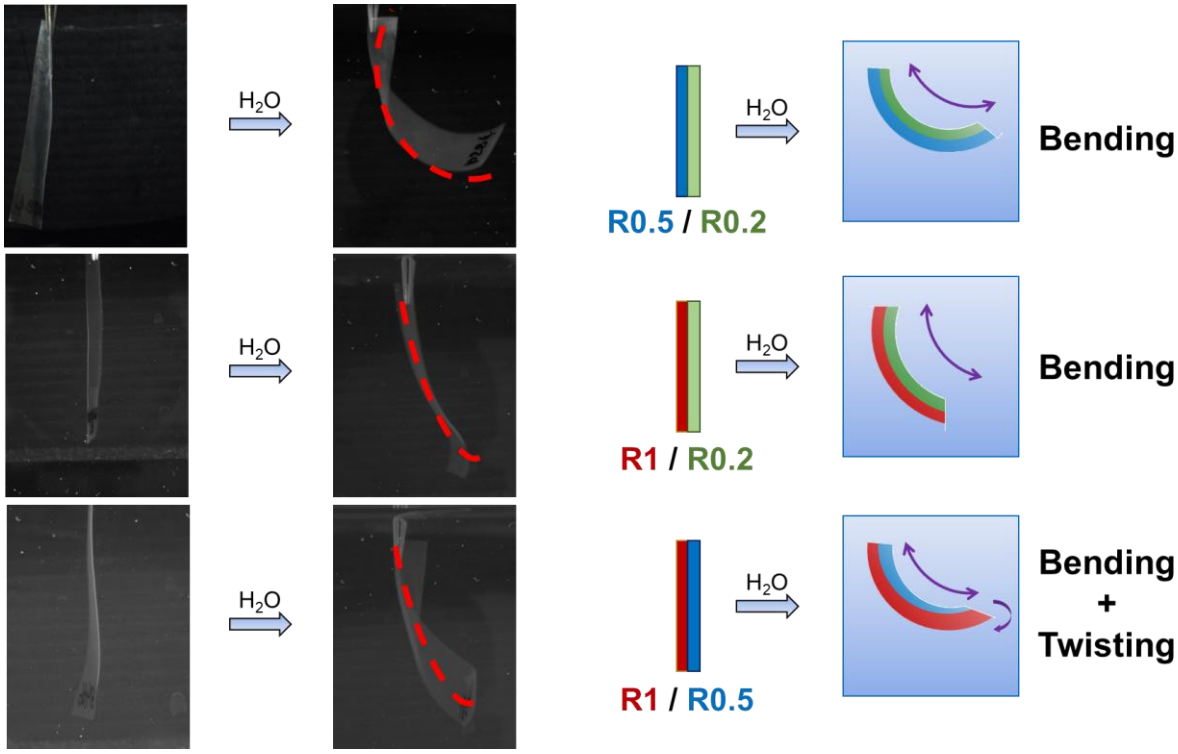

Fig. 5 Photographs showing the bending of R0.5/R0.2, R1/R0.2 and R1/R0.5 films when they were immersed in water at time 0 and 30 min; and schematic illustration of the behavior of the films in water.

The films R0.5/R0.2 and R1/R0.2 showed a simple bending actuation in water, in a higher extent in the case of the R0.5/R0.2 film. Differently, the R1/R0.5 display a more complex behavior

since, both bending and twisting were observed. (Fig 5) According to the water uptake values of starting films (Table 1), the highest difference in swelling between the layers corresponded to the R1/R0.2 film, so the highest bending was expected for this film. Nevertheless, the experimental results indicated a different tendency, and the greater bending was observed for the R0.5/R0.2 film. The bending of bilayer films triggered by the asymmetric expansion of the layers depends not only on the difference in water uptake within the layers, but also on their storage modulus, and the film dimensions and geometry (Le Duigou et al., 2019; Rueggeberg & Burgert, 2015; Wang, Tian, Ras, & Ikkala, 2015; Zhang et al., 2015). In the case of R1, the storage modulus is the lowest measured and is almost 2 decades lower than those of R0.2 which suggest that the difference of mechanical behavior would limit the bending and counteract the anisotropic swelling action. In the case of the R1/R0.5 actuation, the difference in swelling and storage modulus are not that high however, the twisting and bending of the R1/R0.5 film may be justified in terms of the lower thickness of the film (95 µm) compared to the others (122-155 µm). Thus, it is likely that the actuating properties of XG/CNC/Chi films is combination of several parameters and can finely be controlled by the hydrogel composition and film architecture. Further works will be necessary to model and predict the actuating behavior opening the door to the implementation of new soft bio-based materials but also to biomimetic tools to investigate biology related issues such plant cell wall shaping and growth.

4. Conclusions

In this work, we took advantage of the interactions between cellulose, xyloglucan and chitosan to fabricate bio-based hydrogels. The specificity of the cellulose/xyloglucan association and the subsequent formation of a double network by the addition of a charged biopolymer (chitosan)

provided the hydrogel stability. By tuning the XG/CNC ratio, and therefore the adsorption regime of xyloglucan on the cellulose surface, the physical properties of the hydrogel, such as transparency, storage and loss moduli, and water uptake, can be easily modified. The combination of two different XG/CNC ratios in a bilayer film allowed the fabrication of actuators driven by the asymmetric swelling between the layers. This work opens new routes in the field of actuators, we fabricated totally bio-based hydrogels without chemical cross-linking and whose properties and response to stimuli can be tuned by the interactions between the biopolymers.

Acknowledgements

Camille Jonchère and Catherine Garnier are acknowledged for their excellent help for rheology measurements. This work is a contribution to the HOBIT program financed by the Pays de la Loire region.

Declaration of competing interest

The authors declare no conflicts of interest.

Supporting Information.

No supporting material

AUTHOR INFORMATION

Corresponding Author

* bernard.cathala@inrae.fr

Author Contributions

The manuscript was written through contributions of all authors. All authors have given approval to the final version of the manuscript.

References

Benselfelt, T., Cranston, E. D., Ondaral, S., Johansson, E., Brumer, H., Rutland, M. W., & Wagberg, L. (2016). Adsorption of Xyloglucan onto Cellulose Surfaces of Different Morphologies: An Entropy-Driven Process. *Biomacromolecules,* 17(9), 2801-2811.

Benselfelt, T., Engstrom, J., & Wagberg, L. (2018). Supramolecular double networks of cellulose nanofibrils and algal polysaccharides with excellent wet mechanical properties. *Green Chemistry,* 20(11), 2558-2570.

Chang, C. Y., & Zhang, L. N. (2011). Cellulose-based hydrogels: Present status and application prospects. *Carbohydrate Polymers,* 84(1), 40-53.

Chemin, M., Beaumal, B., Cathala, B., & Villares, A. (2020). pH-Responsive Properties of Asymmetric Nanopapers of Nanofibrillated Cellulose. *Nanomaterials,* 10(7), 1380.

Chen, Q., Chen, H., Zhu, L., & Zheng, J. (2015). Fundamentals of double network hydrogels. *Journal of Materials Chemistry B,* 3(18), 3654-3676.

Chen, W., Sun, B., Biehl, P., & Zhang, K. (2022). Cellulose-Based Soft Actuators. *Macromolecular Materials and Engineering,* n/a(n/a), 2200072.

Coviello, T., Matricardi, P., Marianecci, C., & Alhaique, F. (2007). Polysaccharide hydrogels for modified release formulations. *Journal of Controlled Release,* 119(1), 5-24.

Dammak, A., Quemener, B., Bonnin, E., Alvarado, C., Bouchet, B., Villares, A., Moreau, C., & Cathala, B. (2015). Exploring Architecture of Xyloglucan Cellulose Nanocrystal Complexes through Enzyme Susceptibility at Different Adsorption Regimes. *Biomacromolecules,* 16(2), 589-596.

De France, K. J., Cranston, E. D., & Hoare, T. (2020). Mechanically Reinforced Injectable Hydrogels. *Acs Applied Polymer Materials,* 2(3), 1016-1030.

De France, K. J., Hoare, T., & Cranston, E. D. (2017). Review of Hydrogels and Aerogels Containing Nanocellulose. *Chemistry of Materials,* 29(11), 4609-4631.

de Freitas, R. A., Spier, V. C., Sierakowski, M. R., Nicolai, T., Benyahia, L., & Chassenieux, C. (2015). Transient and quasi-permanent networks in xyloglucan solutions. *Carbohydrate Polymers,* 129, 216-223.

Du, H. S., Liu, W. M., Zhang, M. L., Si, C. L., Zhang, X. Y., & Li, B. (2019). Cellulose nanocrystals and cellulose nanofibrils based hydrogels for biomedical applications. *Carbohydrate Polymers,* 209, 130-144.

Eichhorn, S. J. (2011). Cellulose nanowhiskers: promising materials for advanced applications. *Soft Matter,* 7(2), 303-315.

Flory, P. J. (1953). *Principles of Polymer Chemistry*: Cornell University Press.

Hu, Z., Cranston, E. D., Ng, R., & Pelton, R. (2014). Tuning Cellulose Nanocrystal Gelation with Polysaccharides and Surfactants. *Langmuir,* 30(10), 2684-2692.

Hynninen, V., Hietala, S., McKee, J. R., Murtomaki, L., Rojas, O. J., Ikkala, O., & Nonappa. (2018). Inverse Thermoreversible Mechanical Stiffening and Birefringence in a Methylcellulose/Cellulose Nanocrystal Hydrogel. *Biomacromolecules,* 19(7), 2795-2804.

Kishani, S., Benselfelt, T., Wagberg, L., & Wohlert, J. (2021). Entropy drives the adsorption of xyloglucan to cellulose surfaces-A molecular dynamics study. *Journal of Colloid and Interface Science,* 588, 485-493.

Le Duigou, A., Keryvin, V., Beaugrand, J., Pernes, M., Scarpa, F., & Castro, M. (2019). Humidity responsive actuation of bioinspired hygromorph biocomposites (HBC) for adaptive structures. *Composites Part a-Applied Science and Manufacturing,* 116, 36-45.

Lindstrom, T., Wagberg, L., & Larsson, T. (2005). *ON THE NATURE OF JOINT STRENGTH IN PAPER - A REVIEW OF DRY AND WET STRENGTH RESINS USED IN PAPER MANUFACTURING*.

Lombardo, S., Cathala, B., & Villares, A. (2021). Adsorption of biopolymers onto nanocelluloses for the fabrication of hollow microcapsules. *Nordic Pulp & Paper Research Journal,* 36(4), 651-661.

Lombardo, S., & Thielemans, W. (2019). Thermodynamics of Adsorption at Nanocellulose Surfaces. *Abstracts of Papers of the American Chemical Society,* 257.

McCracken, J. M., Donovan, B. R., & White, T. J. (2020). Materials as Machines. *Advanced Materials,* 32(20), 1906564.

Moreau, C., Villares, A., Capron, I., & Cathala, B. (2016). Tuning supramolecular interactions of cellulose nanocrystals to design innovative functional materials. *Industrial Crops and Products,* 93, 96-107.

Pääkkö, M., Ankerfors, M., Kosonen, H., Nykänen, A., Ahola, S., Österberg, M., Ruokolainen, J., Laine, J., Larsson, P. T., Ikkala, O., & Lindström, T. (2007). Enzymatic Hydrolysis Combined with Mechanical Shearing and High-Pressure Homogenization for Nanoscale Cellulose Fibrils and Strong Gels. *Biomacromolecules,* 8(6), 1934-1941.

Park, Y. B., & Cosgrove, D. J. (2015). Xyloglucan and its Interactions with Other Components of the Growing Cell Wall. *Plant and Cell Physiology,* 56(2), 180-194.

Patel, P., & Thareja, P. (2022). Hydrogels differentiated by length scales: A review of biopolymer-based hydrogel preparation methods, characterization techniques, and targeted applications. *European Polymer Journal,* 163.

Revol, J. F., Bradford, H., Giasson, J., Marchessault, R. H., & Gray, D. G. (1992). Helicoidal Self-ordering of Cellulose Microfibrils in A queous Suspension. *International Journal of Biological Macromolecules,* 14(3), 170-172.

Rueggeberg, M., & Burgert, I. (2015). Bio-Inspired Wooden Actuators for Large Scale Applications. *PLoS ONE,* 10(4).

Shang, J. J., Le, X. X., Zhang, J. W., Chen, T., & Theato, P. (2019). Trends in polymeric shape memory hydrogels and hydrogel actuators. *Polymer Chemistry,* 10(9), 1036-1055.

Talantikite, M., Beury, N., Moreau, C., & Cathala, B. (2019). Arabinoxylan/Cellulose Nanocrystal Hydrogels with Tunable Mechanical Properties. *Langmuir,* 35(41), 13427-13434.

Talantikite, M., Gourlay, A., Le Gall, S., & Cathala, B. (2019). Influence of Xyloglucan Molar Mass on Rheological Properties of Cellulose Nanocrystal/Xyloglucan Hydrogels. *Journal of Renewable Materials,* 7(12), 1381-1390.

493 Talantikite, M., Stimpson, T. C., Gourlay, A., Le-Gall, S., Moreau, C., Cranston, E. D., Moran-
494 Mirabal, J. M., & Cathala, B. (2021). Bioinspired Thermoresponsive Xyloglucan-
495 Cellulose Nanocrystal Hydrogels. *Biomacromolecules,* 22(2), 743-753.
496 Toivonen, M. S., Kurki-Suonio, S., Schacher, F. H., Hietala, S., Rojas, O. J., & Ikkala, O.
497 (2015). Water-Resistant, Transparent Hybrid Nanopaper by Physical Cross-Linking with
498 Chitosan. *Biomacromolecules,* 16(3), 1062-1071.
499 Villares, A., Bizot, H., Moreau, C., Rolland-Sabate, A., & Cathala, B. (2017). Effect of
500 xyloglucan molar mass on its assembly onto the cellulose surface and its enzymatic
501 susceptibility. *Carbohydrate Polymers,* 157, 1105-1112.
502 Villares, A., Moreau, C., Dammak, A., Capron, I., & Cathala, B. (2015). Kinetic aspects of the
503 adsorption of xyloglucan onto cellulose nanocrystals. *Soft Matter,* 11(32), 6472-6481.
504 Wang, M., Tian, X., Ras, R. H. A., & Ikkala, O. (2015). Sensitive Humidity-Driven Reversible
505 and Bidirectional Bending of Nanocellulose Thin Films as Bio-Inspired Actuation.
506 *Advanced Materials Interfaces,* 2(7).
507 Wu, Z. L., Moshe, M., Greener, J., Therien-Aubin, H., Nie, Z., Sharon, E., & Kumacheva, E.
508 (2013). Three-dimensional shape transformations of hydrogel sheets induced by small-
509 scale modulation of internal stresses. *Nature Communications,* 4(1), 1586.
510 Zhang, K., Geissler, A., Standhardt, M., Mehlhase, S., Gallei, M., Chen, L., & Thiele, C. M.
511 (2015). Moisture-responsive films of cellulose stearoyl esters showing reversible shape
512 transitions. *Scientific Reports,* 5.
513 Zhao, X., Chen, X., Yuk, H., Lin, S., Liu, X., & Parada, G. (2021). Soft Materials by Design:
514 Unconventional Polymer Networks Give Extreme Properties. *Chemical Reviews,* 121(8),
515 4309-4372.
516 Zhu, Q., Liu, S., Sun, J., Liu, J., Kirubaharan, C. J., Chen, H., Xu, W., & Wang, Q. (2020).
517 Stimuli-responsive cellulose nanomaterials for smart applications. *Carbohydrate*
518 *Polymers,* 235, 115933.
519 Zhu, T., Mao, J., Cheng, Y., Liu, H., Lv, L., Ge, M., Li, S., Huang, J., Chen, Z., Li, H., Yang, L.,
520 & Lai, Y. (2019). Recent Progress of Polysaccharide-Based Hydrogel Interfaces for
521 Wound Healing and Tissue Engineering. *Advanced Materials Interfaces,* 6(17).

522